Macromolecules

pubs.acs.org/Macromolecules Article

A Systematic Study of the Temperature-Induced Performance Decline of *ansa*-Metallocenes for iPP

Christian Ehm,* Antonio Vittoria, Georgy P. Goryunov, Vyatcheslav V. Izmer, Dmitry S. Kononovich, Pavel S. Kulyabin, Rocco Di Girolamo, Peter H. M. Budzelaar, Alexander Z. Voskoboynikov, Vincenzo Busico, Dmitry V. Uborsky,* and Roberta Cipullo*

Cite This: https://dx.doi.org/10.1021/acs.macromol.0c01771 Read Online

ACCESS | Metrics & More | Article Recommendations | Supporting Information

ABSTRACT: Highly accurate high-throughput experimentation (HTE) data for a set of 21 silicon-bridged C_2-symmetric *ansa*-zirconocenes in propene homopolymerization were collected and were used to develop quantitative structure − activity relationship (QSAR) models for several performance indicators at high polymerization temperature (T_p = 100 °C) by using chemically meaningful descriptors. Most notably, stereoselectivity is well described by a two-descriptor model linking the quadrant model for stereoselectivity (sterics) with the chain epimerization model (electronics). The catalysts show widely varying temperature responses, most notably on stereoselectivity and molar mass capability, while the regioselectivity response is uniformly weak. Soft conformational locks lose their performance rapidly while hard conformational locks offer enhanced performance even at high temperatures. The quest for high-temperature stable, well-performing *ansa*-zirconocenes will unquestionably lead to systems with enhanced rigidity.

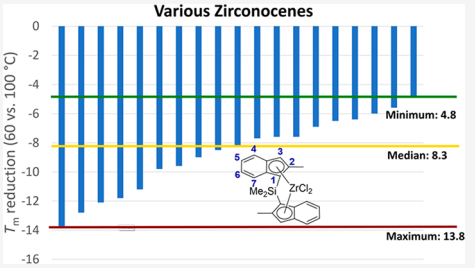

INTRODUCTION

Known since the 1950s,[1,2] metallocenes did not gain traction as a platform for the industrial production of polyolefin resins until the mid-1970s when Kaminsky and Sinn introduced a superior activator, methylaluminoxane (MAO).[3−6] The boost in activity observed with MAO started a metallocene research frenzy in both academia and industry that involved nearly all polyolefin companies active at that time and hundreds of academic laboratories worldwide.[7−12] As single-center polymerization catalysts, metallocenes allow "easy" identification of structure/property correlations and thus precision tuning of the active pocket.[13−18] Indeed, one of the most important contributions of metallocene research to the science of olefin polymerization catalysis came in the form of mechanistic understanding, from the origins of enantioselectivity[18−21] to factors determining molecular weight[22] or dormancy and catalyst activity.[15,23−28]

Market penetration for metallocenes took longer than anticipated,[8] the hype died down along with it, and the focus shifted to non-metallocene systems.[29,30] Nevertheless, metallocenes nowadays occupy a sizable market position in the area of linear low-density polyethylene (mLLDPE) due to distinct advantages over traditional Ziegler−Natta resins, for example, higher clarity and impact strength.[8] Conversely, isotactic polypropylene (iPP) resins are still dominated by Ziegler−Natta catalysts,[11,12,31−33] and metallocene-based resins represent only a specialty niche.[7,9,34]

Gas- and slurry-phase processes, in which the catalyst is immobilized on a solid support, dominate the industrial production of polyolefins.[35] However, homogeneous solution processes can offer greater operational flexibility and wider product ranges.[36] Polymer precipitation adversely affects solution processes, imposing demanding restrictions to high operating temperatures, which in turn leads to challenging requirements for the catalyst: high thermal stability and high selectivity even at elevated temperatures.[35] The challenge has been solved for mLLDPE, but propene polymerization proved to be much more problematic.[36]

The performance of C_2-symmetric *ansa*-zirconocenes for iPP deteriorates rapidly with decreasing monomer concentration and increasing temperature.[37−42] The scientific community at large views these catalysts as fully optimized with little to no room for further improvement.[43] This being said, industry has never really given up on the dream of increasing the operational temperature window of metallocenes to levels appropriate for commercial solution type processes. In particular, both Basell/Borealis[42,44−47] and Exxon[48] revealed *ansa*-zirconocene catalysts with improved high-temperature performance in the past decade.

Likely due to the scarcity of catalysts with good high-temperature performance, larger systematic studies on C_2-

Received: July 29, 2020
Revised: October 4, 2020

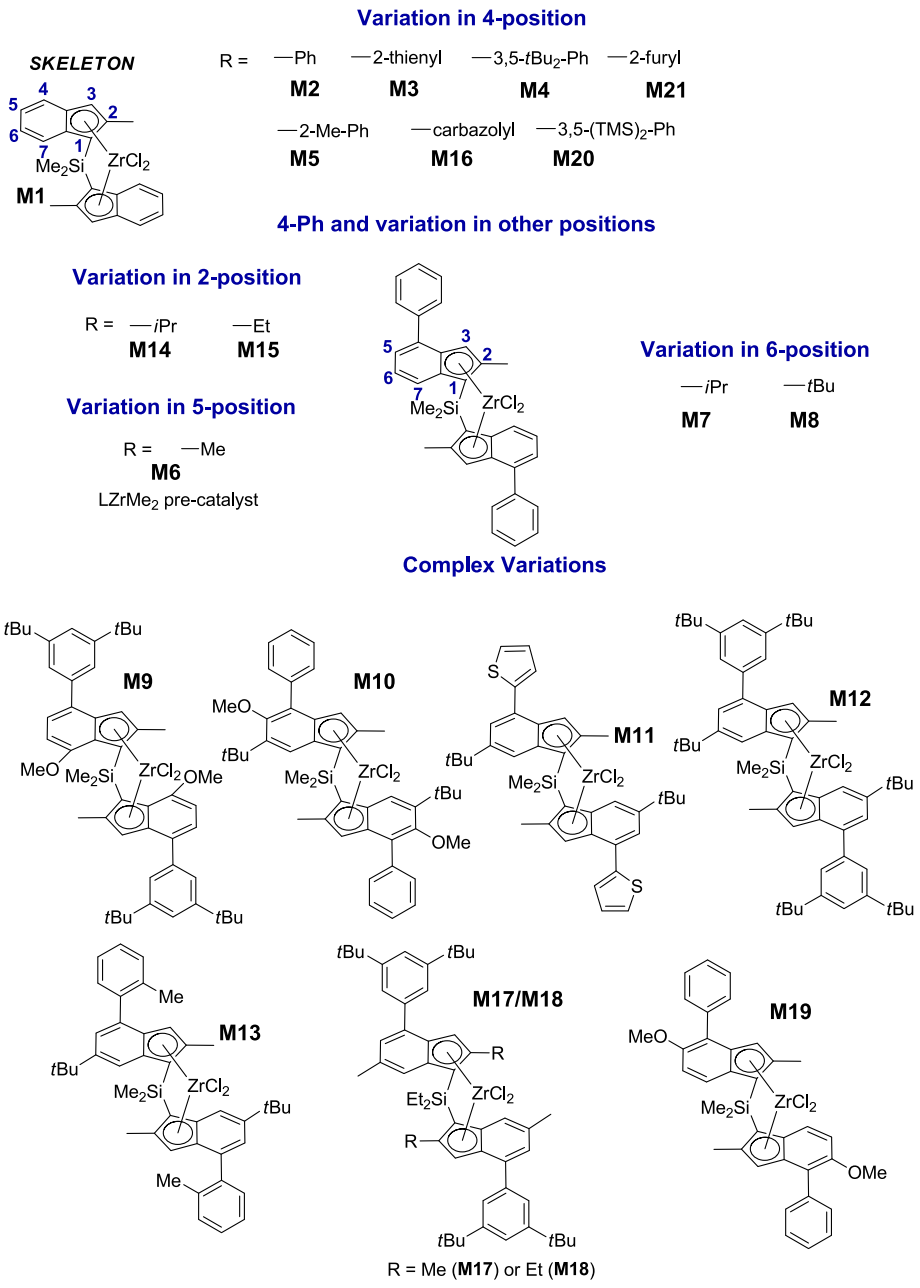

Figure 1. Precatalysts **M1**−**M21** screened in propene polymerization at T_p = 100 °C and $p(C_3H_6)$ = 7.9 bar. For additional experimental details see Table 1 and the Supporting Information.

symmetric *ansa*-zirconocenes aimed to understand the main features of a well-working high-temperature performance catalyst are to our knowledge unavailable. Aggravating is the fact that polymerization performance depends crucially on the polymerization conditions. For example, the reported performance of Spaleck's seminal *rac*-Me_2Si(2-Me-4-Ph-indenyl)$_2ZrCl_2$ precatalyst[49] at higher polymerization temperatures varies tremendously and inexplicably (see Table S4 of the Supporting Information).[36,42,44,48] For T_p = 100 °C, for example, molar mass capabilities varying by a factor of 6 (M_w 40−246 kDa) have been reported, while melting points vary by 10 °C (145−155 °C)!

Recently, we reported a sizable high-throughput experimentation (HTE) and predictive quantitative structure−activity relationship (QSAR) modeling study focusing on *ansa*-zirconocene catalysts for iPP.[50,51] Of the 40 tested catalysts, 17 showed M_w over 1 MDa at 60 °C, thus providing a solid base for a high-temperature screening.

In the following, the results of a screening of 21 *ansa*-zirconocene catalysts for iPP at 100 °C are presented. The data are analyzed with regard to the observed performance decline at high temperatures. "White-box" QSAR models based on chemically meaningful descriptors and trend analyses allow the identification of design principles for catalysts with improved high-temperature performance.

EXPERIMENTAL SECTION

Catalyst Synthesis. **M1** and **M2** were kindly donated by SABIC and used as received. **M3**,[52] **M4**,[53] **M5** and **M21**,[50] **M9**,[54] **M10**,[44] **M15**,[55] **M16**,[48] and **M6**−**M8**, **M11**−**M14**, and **M17**−**M20**[51] were synthesized according to the literature.

https://dx.doi.org/10.1021/acs.macromol.0c01771
Macromolecules XXXX, XXX, XXX−XXX

Table 1. Results of the Characterization of PP Samples Prepared at T_p = 100 °C and $p(C_3H_6)$ = 7.9 bar in Toluene with the 21 *ansa*-Zirconocene Catalysts of Figure 1 (See Text for Details)[a]

		100 °C								60 °C[b]				
ID	substituent pattern	2,1	3,1	$regio_{tot}$[c]	1-σ[d]	M_n[e]	PDI	R_p[f]	T_m[g]	$regio_{tot}$[c]	1-σ[d]	M_n[e]	PDI	T_m[g]
M1	2-Me	0.08(3)	0.28(3)	0.36	4.80(20)	6	2.2	66	n.d.	0.29	1.35	100	1.9	145.7
M2	2-Me-4-Ph	0.25	0.17	0.41	0.41	27	2.0	32	150.4	0.32	0.12	320	2.0	160.2
M3	2-Me-4-(2-thienyl)	0.33	0.37	0.60	1.00	17	2.0	58	141.4	0.50	0.29	230	2.0	153.2
M4	2-Me-4-(3,5-tBu$_2$Ph)	0.21	0.09	0.30	0.18	60	2.0	136	153.9	0.17	0.06	530	2.2	162.4
M5	2-Me-4-(2-MePh)	0.19	0.33	0.52	0.19	48	1.9	14	152.2	0.42	0.02	470	1.8	158.2
M6	2,5-Me-4-Ph	0.35	0.29(3)	0.64	0.07	52	2.1	77	153.4	0.48	0.02	610	2.1	158.2
M7	2-Me-4-Ph-6-iPr	0.35	0.35(3)	0.70	0.34(3)	48	2.0	149	148.5	0.54	0.10	630	2.3	156.1
M8	2-Me-4-Ph-6-tBu	0.41	0.40	0.81	0.35	85	2.1	94	146.5	0.69	0.11	710	2.4	153.4
M9	2-Me-4-(3,5-tBu$_2$Ph)-7-OMe	0.29	0.14	0.43	0.10	44	2.0	172	154.6	0.23	0.03	400	2.2	162.2
M10	2-Me-4-Ph-5-OMe-6-tBu	0.57	0.42	0.99	0.06	161	2.2	23	149.5	0.71	0.02	1400	2.3	156.0
M11	2-Me-4-(2-thienyl)-6-tBu	0.66	0.55	1.21	0.72	67	1.9	28	139.0	1.05	0.31	620	2.3	148.0
M12	2-Me-4-(3,5-tBu$_2$Ph)-6-tBu	0.35	0.14	0.49	0.14	109	2.2	96	152.3	0.30	0.05	950	2.3	160.6
M13	2-Me-4-(2-MePh)-6-tBu	0.31	0.7	1.01	0.15	85	2.1	38	148.7	0.83	0.02	990	2.3	154.3
M14	2-iPr-4-Ph	n.d.	n.d.	n.d.	8.00	1	1.8	6	n.d.	0.09	2.80	19	2.3	137.2
M15	2-Et-4-Ph	0.13	0.15	0.28	0.65	18	1.9	74	147.7	0.21	0.11	220	2.1	160.5
M16	2-Me-4-(*N*-carbazolyl)	0.16	0.12	0.28	0.21	74	2.1	13	155.1	0.20	0.04	800	2.3	161.5
M17	2-Me-4-(3,5-tBu$_2$Ph)-6-Me	0.22	0.13	0.35	0.23	72	1.9	89	150.1	0.18	0.04	740	2.3	162.2
M18	2-Et-4-(3,5-tBu$_2$Ph)-6-Me	0.11	0.16	0.27	0.33	40	2.0	189	153.5	0.11	0.04	620	2.4	163.1
M19	2-Me-4-Ph-5-OMe	0.28	0.22	0.50	0.14	51	2.0	160	152.0	0.35	0.04	760	2.1	159.7
M20	2-Me-4-(3,5-TMS$_2$Ph)	0.22	0.15	0.37	0.29	57	1.9	159	150.4	0.20	0.05	550	2.2	161.6
M21	2-Me-4-(2-furyl)	0.63	0.35	0.98	2.50	9	2.4	10	129.4	0.91	0.80	130	2.1	143.2

[a] T_p = 60 °C, $p(C_3H_6)$ = 6.6 bar data provided for comparison. Experimental conditions: T_p = 100 °C, $p(C_3H_6)$ = 7.9 bar, solvent toluene, scavenger Al(iBu)$_3$, activator TTB (for abbreviations see text), [TTB]/[Zr] = 10. Experimental uncertainty is ±2 on last significant digit for 1-σ and $regio_{tot}$, unless otherwise indicated in parentheses; ±20% on M_n. For more details see Tables S1 and S2. [b] 60 °C data taken from refs 50 and 51. [c] Total fraction of 2,1 and 3,1 monomeric units in % (^{13}C NMR). [d] Fraction of stereoirregular monomeric units in % (^{13}C NMR), according to the enantiomorphic-site statistical model.[18] [e] In kDa. [f] In kg mmol$_{Zr}^{-1}$ h^{-1}. [g] In °C. PDI = polydispersity index (M_w/M_n). n.d.: not determined; the catalyst produced oligomers under the used conditions.

Polymer Synthesis and Characterization. All polymerization experiments were performed in toluene in a Freeslate Parallel Pressure Reactor setup with 48 reaction cells (PPR48), fully contained in a triple MBraun glovebox under nitrogen. The cells (5.0 mL working volume) feature 800 rpm magnetically coupled stirring and individual online reading/control of temperature, pressure, monomer uptake, and uptake rate. The setup and the operating protocol are described in full detail in refs S6 and S7 and the Supporting Information and have been used successfully in various homogeneous and heterogeneous polymerization studies.[50,51,58−64] Polymerization conditions were as follows: T = 100 °C; $p(C_3H_6)$ = 7.9 bar; scavenger = Al(iBu)$_3$ (10 μmol), activator [trityl]$^+$[B(C_6F_5)$_4$]$^-$ (TTB), and [TTB]/[Zr] = 10.[65] The dichloride precatalysts were injected into the PPR cells without preactivation. The following injection sequence was used with individual solutions separated by nitrogen gas caps in the injection needle: (1) toluene "buffer", (2) toluene activator solution, (3) catalyst solution, and (4) toluene "chaser". All experiments were performed at least in duplicate. The monomer was fed on demand.

The polymers were characterized by (a) high-temperature GPC with a Freeslate Rapid-GPC setup, (b) quantitative ^{13}C NMR with a Bruker DRX 400 spectrometer equipped with a high-temperature cryoprobe (for 5 mm O.D. tubes) and a preheated robotic sample changer, and (c) DSC with a Mettler Toledo DSC-822 calorimeter. Polymer melting points (T_m) were collected from the second heating scan. All results are averages on polymer samples produced in polymerization experiments performed in duplicate. More details can be found in Tables S1 and S2.

Computational Details. Geometries of metallocene dichlorides were fully optimized by using the Gaussian 16 software package[66] in combination with the OPTIMIZE routine of Baker[67,68] and the BOpt software package.[69] Following the protocol proposed in ref 70, all precatalysts were optimized at the TPSSTPSS[73]/cc-pVDZ(-PP)[72−74] level of theory by using a small core pseudopotential on Zr.[75,76] The protocol has been successfully used, in combination with M06-2X[77] single-point energy corrections, to address several polymerization-related problems: absolute barrier heights for propagation,[78] comonomer reactivity ratios,[79,80] metal−carbon bond strengths under polymerization conditions,[81−83] electronic and steric tuning of molar mass capability,[84] and QSAR modeling.[50,51,62,63] The density fitting approximation (Resolution of Identity, RI)[85−88] and standard Gaussian16 quality settings [Scf = Tight and Int(Grid = Ultrafine)] were used at the optimization stage and for single-point energy (SP) calculations. All structures represent true minima (as indicated by the absence of imaginary frequencies). Buried volume descriptors were calculated by using the SambVca 2.0 program.[89] NPA charges were determined from SP calculations at the M06-2X/cc-pVTZ(-PP) level of theory using the NBO 3.1 program,[90] implemented in Gaussian 16.

RESULTS AND DISCUSSION

Experimental Screening. The 21 "Spaleck" type zirconocenes screened in propene homopolymerization (Figure 1) at 100 °C were previously tested also at 60 °C.[50,51] All dichloride precatalysts were used as pure *rac*-isomers. For **M6**, a dimethyl precursor was used, as the dichloride precursor could not be sufficiently purified.[51] HTE polymerizations were performed on a PPR48 platform in toluene under a standard set of conditions; see the Experimental Section and the Supporting Information for details. All samples were characterized with GPC for molecular weight determination and ^{13}C NMR spectroscopy for microstructural analysis by using specifically implemented HTE protocols.[56,57]

https://dx.doi.org/10.1021/acs.macromol.0c01771
Macromolecules XXXX, XXX, XXX−XXX

General Experimental Trends. The results of the screening of **M1**−**M21** are summarized in Table 1; detailed polymerization results can be found in Table S1. Catalyst stereoselectivity (σ, i.e., probability of monomer insertions with the preferred enantioface) ranged between 0.9200 and 0.9994 (i.e., 1-σ spanned from 8.0 to 0.06% stereoirregular monomeric units in the polymer). Overall regioselectivity ($regio_{tot}$, i.e., the summed mole fractions of monomer insertions with 2,1 or 3,1 enchainments) ranged between 0.9879 and 0.9973 (i.e., from 1.21 to 0.27 mol % regioirregular monomeric units);[91] the number-average polymer molar mass (M_n) was between 1 and 160 kDa. Melting points were in the order of 139.0−155.1 °C, with two polymers being too short to crystallize (**M1** and **M14**). Compared to results obtained at 60 °C,[50,51] stereoerrors typically increase by a factor of 3.4, regioerrors increase only by a factor of 1.3, and molar mass capability is most dramatically affected and typically drops by a factor of 11.6 (see Table 2). Melting points decrease typically by 8 °C.

Superficially, one can expect that a catalyst with good performance at lower temperature also delivers a respectable performance at higher temperature. However, the individual responses of the various catalysts to the temperature change differ markedly. This is emphasized when looking at the response ranges (Table 2): (i) $regio_{tot}$ increase by a factor of 1.1−2.5, (ii) 1-σ increase from as little as 2.3-fold up to 9.5-fold, (iii) M_n decreases between 8.4- and 19-fold, and (iv) most notably, the melting point, T_m, decreases by 4.8 to 13.8 °C. The influence of individual substituents on stereoselectivity, regioselectivity, and molar mass capability of C_2-symmetric *ansa*-zirconocenes at 60 °C has been discussed at length recently.[51] In the following, we will therefore focus on the experimental temperature response of different substituent patterns (see also Table 2).

Regioselectivity. The regioselectivity of most catalysts is nearly temperature independent and decreases only very slightly (1.1−1.4-fold) with increasing temperature. This decrease amounts to less than would be expected solely based on the RT factor. In fact, $\Delta\Delta G^{\ddagger}_{regio}$ increases by ≈0.2 kcal/mol for most catalysts (see Table S2). Only one substituent pattern, 4-(3,5-R_2Ph), present in catalysts **M4**, **M9**, **M12**, **M17**, **M18**, and **M20**, leads to a markedly higher increase in regioerrors going from 60 to 100 °C (1.6−2.5-fold, Table 2). Resconi has even noted an increased regioselectivity with increased temperature for the catalysts **M2** and **M10** in the temperature range 30−85 °C, albeit his systems were immobilized.[42]

Stereoselectivity. Several substituent patterns appear temperature sensitive. Increasing the polymerization temperature leads to a marked decrease in stereoselectivity for catalysts with a 4-(2-MePh) substituent (**M5** and **M13**, 7.5−9.5-fold increase of stereoerrors), a 2-Et substituent (**M15** and **M18**, 5.8−8.3-fold increase), 4-(*N*-carbazolyl) (**M16**, 5.3-fold), and 4-(3,5-TMS_2Ph) (**M20**, 5.8-fold). Poorly stereoregular catalysts **M1** (4-H), **M3** (4-(2-thienyl)), and **M14** (2-*i*Pr) also show a high temperature sensitivity (Table 2, footnote, and Table S3).

Conversely, electron-donating substituents in the 5- or 6-position like Me, *i*Pr, *t*Bu, and OMe (in **M6**, **M7**, **M8**, and **M10**−**M13**) lead to a smaller than typical worsening of the stereoselectivity going from 60 to 100 °C.

The marked decrease of stereoselectivity with increasing temperature is well-known and due to the occurrence of chain epimerization competing with monomer insertion.[18,21,37,92−94]

Table 2. Temperature Effects; Increase (IF) or Decrease Factors (DF) for Metallocenes M1−M21 for Polymerization at 100 vs 60 °C

ID	substituent pattern	$regio_{tot}$ IF[a]	1-σ IF[a]	M_n DF[b]	T_m[c] decrease	T effects[d]
M1	2-Me	1.2	(3.6)*	16.7	N/A	-
M2	2-Me-4-Ph	1.3	3.4	11.9	9.8	-
M3	2-Me-4-(2-thienyl)	1.2	(3.4)*	13.5	11.8	-
M4	2-Me-4-(3,5-tBu$_2$) Ph	1.8	3.0	8.8	8.5	-
M5	2-Me-4-(2-Me)Ph	1.2	9.5	9.8	6.0	-
M6	2,5-Me-4-Ph	1.3	3.5	11.7	4.8	+
M7	2-Me-4-Ph-6-*i*Pr	1.3	3.4	13.1	7.6	-
M8	2-Me-4-Ph-6-*t*Bu	1.2	3.2	8.4	6.9	+
M9	2-Me-4-(3,5-tBu$_2$) Ph-7-OMe	1.9	3.3	9.1	7.6	-
M10	2-Me-4-Ph-5-OMe-6-*t*Bu	1.4	3.0	8.7	6.5	+
M11	2-Me-4-(2-thienyl)-6-*t*Bu	1.2	2.3	9.3	9.0	+
M12	2-Me-4-(3,5-tBu$_2$) Ph-6-*t*Bu	1.6	2.8	8.7	8.3	-
M13	2-Me-4-(2-Me) Ph-6-*t*Bu	1.2	7.5	11.6	5.6	-
M14	2-*i*Pr-4-Ph	N/A	(2.9)*	19.0	N/A	-
M15	2-Et-4-Ph	1.3	5.9	12.2	12.8	- - -
M16	2-Me-4-(*N*-carbazolyl)	1.4	5.3	10.8	6.4	-
M17	2-Me-4-(3,5-tBu$_2$) Ph-6-Me	1.9	5.8	10.3	12.1	- - -
M18	2-Et-4-(3,5-tBu$_2$) Ph-6-Me	2.5	8.3	15.5	9.6	- - -
M19	2-Me-4-Ph-5-OMe	1.4	3.5	14.9	7.7	-
M20	2-Me-4-(3,5-TMS_2)Ph	1.9	5.8	9.6	11.2	- -
M21	2-Me-4-(2-furyl)	1.1	(3.1)*	14.4	13.8	-
median		1.3	3.4	11.6	8.0*	
range		1.2−2.5	2.3−9.5	8.4−19.0	4.8−12.8	

[a]Calculated as error(100 °C)/error(60 °C). [b]Calculated as M_n(60 °C)/M_n(100 °C). [c]In °C; - = one strong negative temperature dependence, - - = two strong negative temperature dependences, - - - = three strong negative temperature dependences, + no strong negative temperature dependence. [d]**M1**, **M14**, and **M21** (M_n 1−9 kDa) not included. *In a strict sense, one should not compare increase factors (IF) but energy changes, which however is less intuitive. Table S3 shows the changes expressed in terms of $\Delta\Delta G^{\ddagger}$; this does not affect the observed trends, except for the four poorly stereoregular catalysts **M1**, **M3**, **M14**, and **M21**, which according to the IF show average temperature sensitivity but in terms of $\Delta\Delta G^{\ddagger}$ are in fact more temperature sensitive.

To confirm that this is also the case here, catalysts **M8**, **M10**, and **M18** were also tested at a lower propene pressure (see Table S1).

Molar Mass Capability. Bulky 2-R substituents like ethyl and isopropyl, present in **M14**, **M15**, and **M18**, lead to a more dramatic performance drop (12−19-fold, Table 2) as do the simple 4-position substituents H (**M1**), Ph (**M2**), 2-thienyl (**M3**), and 2-furyl (**M21**) (without any other substituents around the indenyl core). 5-OMe substitution (**M19**, 15-fold drop) and 6-*i*Pr substitution (**M7**, 13-fold drop) also show high temperature sensitivity. Conversely, 4-(3,5-R_2Ph) (**M4**, **M9**, **M12**, **M17**, and **M20**), 6-*t*Bu (**M8**, **M11**, **M12**, and **M13**), 4-(2-MePh) (**M5** and **M13**), and 4-(*N*-carbazolyl) (**M16**)

https://dx.doi.org/10.1021/acs.macromol.0c01771
Macromolecules XXXX, XXX, XXX−XXX

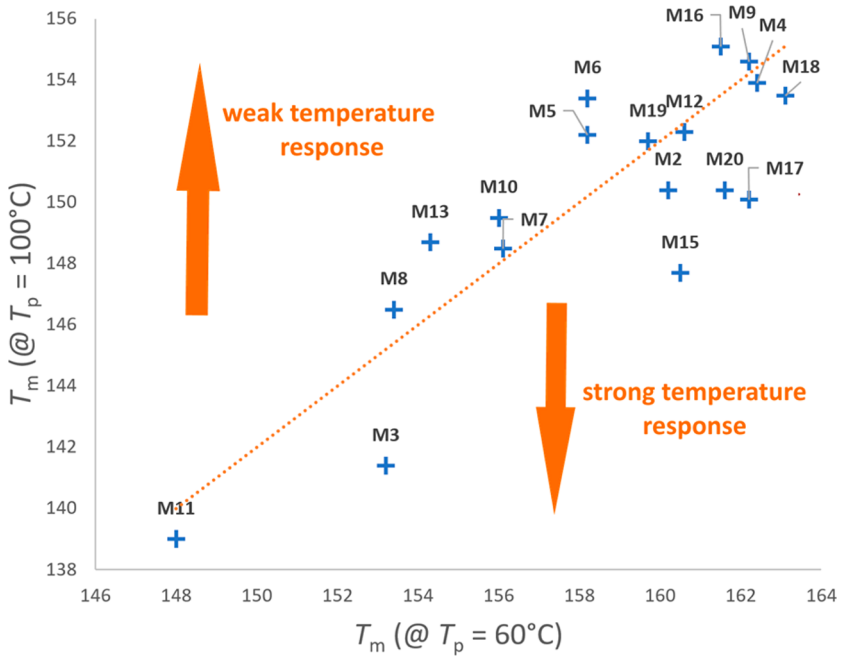

Figure 2. Temperature response of the catalyst set in terms of T_m reduction. The orange line is not a correlation but shows expected behavior if all catalysts would show the median reduction of 8 °C ($T_{m,60°C}-T_{m,100°C}$, see Table 2). Catalysts below the line show a stronger (negative) response, and catalysts above the line show a weaker temperature response. **M1**, **M14**, and **M21** (M_n 1−9 kDa) are not included.

show better than typical temperature performance (8.4−11.6-fold drop).

Control experiments for catalysts **M1**, **M2**, **M4**, **M8**, **M13**, and **M18** showed that reducing the amount of Al(*i*Bu)$_3$ scavenger from 10 to 2.5 μmol did not affect M_n, indicating that chain transfer to aluminum does not play a dominant role, even at elevated temperatures. Additionally, in the ^{13}C NMR spectra of the polymers produced at 100 °C, no evidence of isobutyl chain ends arising from irreversible *trans*-alkylation was found.

Melting Temperature. The melting temperature reflects the amount of microstructural defects in the polymers.[95−98] In several cases, however, the polymer becomes so short (M_n < 20 kDa) that additional effects from the polymer chain length, lowering the T_m, cannot be excluded (**M1**, **M3**, **M14**, **M15**, and **M21**). Most notable is the stark performance decrease observed for the highly optimized catalysts **M17** and **M18** (12.1 and 9.6 °C T_m drop, respectively) as well as for **M20**. This is in line with the fact that stereo- and regioselectivity of these catalysts simultaneously show a strong temperature dependence (see Table 2 and Figure 2). Only moderately sensitive to temperature effects, on the other hand, is the performance of **M5**, **M6**, **M10**, **M13**, and **M16** (4.8−6.5 °C T_m drop).

QSAR Modeling. Recently, we have introduced QSAR models with predictive capability for the iPP performance indicators stereoselectivity, regioselectivity, and molar mass capability at 60 °C.[51] These models are based on a set of seven descriptors that are intuitively related to simple electronic or steric properties of neutral LZrCl$_2$ precatalysts (Figure 3 and Table 3). They are easy to quantify with DFT methods and Cavallo's SambVca program.[89,99,100] Six 3D steric descriptors are used to screen different regions of space around the catalyst (D1-D6), which were selected based on well-established structures of olefin insertion and chain transfer transition states for iPP catalysis. The charge on the metal was found to perform satisfactorily as electronic parameter (D7). The development and the roles of the different descriptors are discussed in detail in ref 51; an overview is shown in Figure 3, Table 3, and Table S5.

We were curious to see whether this descriptor set would also allow to build models for the high temperature performance easily. The set of 21 catalysts, **M1**−**M21**, was divided into two parts. **M1**−**M16** formed the training set, while **M17**−**M21** formed the validation set. **M17**−**M20** were also part of the validation set in ref 51. Linear combinations of the descriptors shown in Figure 3 were tested to reproduce the performance properties of interest (quantified in terms of $\Delta\Delta G^{‡}$ between the relevant competing events; see eqs S1−S3 and Table S6 of the Supporting Information) for the 16 catalysts in the training set.

In the case of regioselectivity and molar mass capability, the models generated at 60 °C[51] just needed to be retrained for 100 °C. The accuracy of the regioselectivity model—which uses the descriptors D2 and D4−D7 at both temperatures—increases, as judged by the coefficient of determination R^2, from $R^2_{60°C}$ = 0.85 to $R^2_{100°C}$ = 0.94 (Figure 4B). The molar mass capability model uses the descriptors D1 and D3−D5 and thus one descriptor fewer than required at 60 °C. D6, which is needed at 60 °C, measures the openness of the "open" quadrant and is not needed for the present data set, as no catalysts with obstructed "empty" quadrant are present. The accuracy at both temperatures is similar to $R^2_{60°C}$ = 0.96 and $R^2_{100°C}$ = 0.98 (Figure 4C).

At 60 °C, the contribution of chain epimerization[18,21,37,92−94] was found to be negligible.[37,50,92] Cavallo has demonstrated that the difference in the fraction of hindered volume between open and closed quadrants (D1) can be used to predict the stereoselectivity of prototypical propene polymerization catalysts belonging to different families.[99] In recent studies, we found that for the present class of catalysts accurate and fine predictions are possible,

https://dx.doi.org/10.1021/acs.macromol.0c01771
Macromolecules XXXX, XXX, XXX−XXX

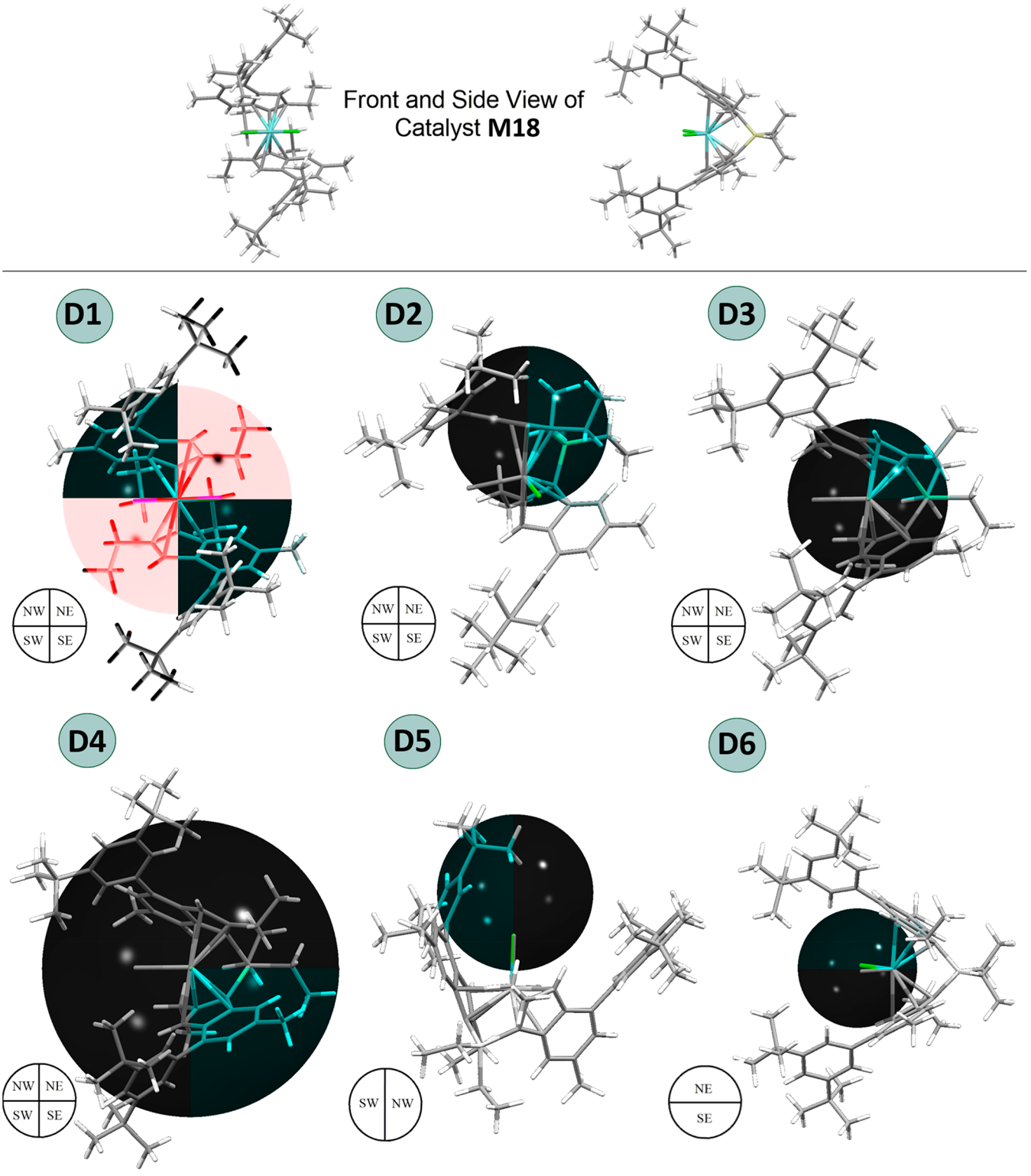

Figure 3. Computational descriptor pool for C_2-symmetric zirconocenes in propene homopolymerization (see also Table 3). Catalyst **M18** used for visualization. D1−D6 were calculated by using Cavallo's SambVca 2.0 program.[89,99,100] Sphere position and size are shown in black; quadrants that are used for descriptor determination are indicated by the blue color of the catalyst backbone, and unused quadrants show grayed-out backbone. For D1 a quadrant difference is used between the occupied (black) and "empty" quadrants (red). D1−D4 are shown so the reader looks along the *z*-axis of the sphere (see Table S5) and so that the colored quadrant matches the description in Table 3. D5 and D6 have been rotated for clarity so that the reader looks across the *z*-axis; in this case only two of the quadrants are visible. Quadrant orientation is shown on the left side of the structures. D7 (charge on metal) is the only electronic descriptor tested. Reproduced with permission from ref 63. Copyright 2020 Royal Society of Chemistry.

provided that the calculation protocol for D1 is customized.[50,51] This correlation should only be valid when stereoselectivity is solely determined by the enantioselectivity of the catalyst, that is, in the absence of chain epimerization.

https://dx.doi.org/10.1021/acs.macromol.0c01771
Macromolecules XXXX, XXX, XXX−XXX

Table 3. Description of the Computational Descriptors

no.	descriptor details and notes
D1	the difference in hindered volume (%V_{Bur}) between open and occupied quadrants of a 5.0 Å sphere centered on Zr
D2	the sum of hindered volumes in NE and SE quadrants of a 3.5 Å sphere centered on C3 (note: this descriptor accounts for the distribution of overall steric bulk at the 2- and 3-position of the indenyl fragment)
D3	the hindered volume in the NE quadrant of a 3.5 Å sphere centered on Cl (note: this descriptor accounts for the fraction of overall steric bulk at the 2- and 3-position of the indenyl fragment oriented toward the active site)
D4	the hindered volume in the SE quadrant of a 6.5 Å sphere centered on Cl (note: this descriptor accounts for the steric bulk contributions from remote 5- and 6-position of the indenyl fragment)
D5	the hindered volume in the SW quadrant of a 3.5 Å sphere centered 2.0 Å away from the Cl atom on an extension of the Zr−Cl bond (Note: this descriptor accounts for remote steric bulk originating from the substituent at 4-position)
D6	the hindered volume in NE (or SW) quadrant of a 3.0 Å sphere centered 1.5 Å in front of the Zr atom (note: this descriptor measures the steric bulk in the open quadrants)
D7	the NPA charge on the $ZrCl_2$ fragment [$q_{ZrCl2,NPA}$]

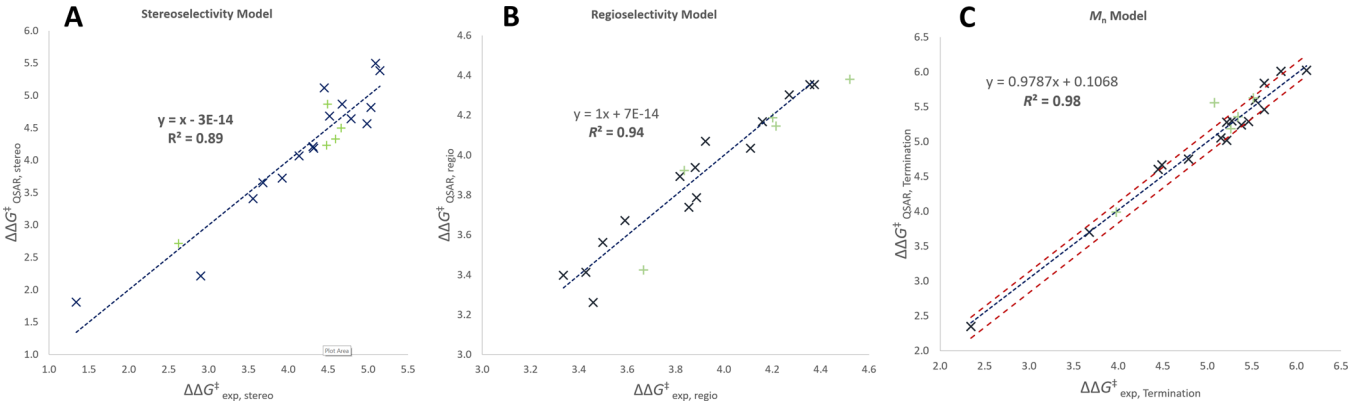

Figure 4. (A−C) QSAR-predicted vs observed $\Delta\Delta G^{\ddagger}$ values (in kcal/mol) for the catalyst training set **M1−M16** (Figure 1 and Table 1, blue crosses): stereoselectivity (A); regioselectivity (B); polymer molar mass capability (C). The catalyst validation set **M17−M21** is displayed by using green plusses. For molar mass capability, error bars (red dotted lines) reflect experimental uncertainty (see Table 1).

In line with these arguments, we found that when D1 is used as the sole descriptor for stereoselectivity, $R^2_{60°C}$ = 0.92 drops to $R^2_{100°C}$ = 0.84 (see Figure S1 for details). This accuracy drop can largely be recovered by using additionally the electronic descriptor D7, the NPA charge on the $ZrCl_2$ fragment. This two-descriptor model gives $R^2_{100°C}$ = 0.89 (Figure 4A). One should note here that for the catalysts **M2−M16**, that is, the catalysts with 4-R ≠ H, a decent single descriptor correlation between D7 and stereoselectivity can be observed ($R^2_{100°C}$ = 0.68, Figure S2).

Key model assessment criteria, that is, the coefficient of determination (R^2), the adjusted coefficient of determination (adj R^2), and cross-validated R^2 via leave-one-out analysis (q^2),[101,102] can be found in Table 4. The mean average deviation from experiment (MAD) and root mean square error (RMSE) values are very low (∼0.07 and ∼0.11 kcal/mol, respectively) for regioselectivity and molar mass capability. The model for stereoselectivity, unsurprisingly (*vide infra*), has a more significant margin of error (0.27 kcal/mol). The model equations and further details can be found in the Supporting Information (eqs S4−S6 and Tables S6−S18).

Table 4. Key QSAR Model Assessment Criteria

	1-σ^a	$regio_{tot}{}^b$	M_n (kDa)
data range (DR)	8.0−0.06	1.21−0.27	1−161
DR (kcal/mol)	3.7	1.1	3.7
R^2/adj R^2	0.89/0.87	0.94/0.90	0.98/0.97
max p value	0.04	9×10^{-3}	4×10^{-3}
q^2	0.60	0.83	0.96
MAD (kcal/mol)	0.27	0.07	0.11
RMSE (kcal/mol)	0.33	0.09	0.13

[a]Fraction of stereoirregular monomeric units in % (^{13}C NMR), according to the enantiomorphic-site statistical model.[18] [b]Total fraction of 2,1 and 3,1 monomeric units in % (^{13}C NMR).

The predictions for the catalyst validation set **M17−M21** are very good, with the sole exception being molar mass capability for **M18**, which is somewhat overestimated (see Table S12).

Challenges of Modeling Chain Epimerization Contributions to Stereoselectivity of Polymerization Catalysts. It has long been noted that the success of a polymerization catalyst hinges not only on its intrinsic selectivity but also on its ability to suppress unwanted side reactions. For stereoselectivity, for example, catalysts with similar enantioselectivity can show dramatically different performance at higher temperature due to a varying vulnerability to chain epimerization.[38] The data in Tables 1 and 2 for catalysts **M1−M21** indicate that for some catalysts chain epimerization does not play a significant role, even at 100 °C, at least at $p(C_3H_6)$ = 7.9 bar. For example, $\Delta\Delta G^{\ddagger}_{enantio}$ at both 60 and 100 °C is nearly identical for **M10−M12** (see Table S3). Several other catalysts, most notably **M5** and **M18**, show such stark performance losses that chain epimerization is likely the culprit and has kicked in early. The other systems present a continuum between these two extremes. The QSAR model for stereoselectivity penalizes catalysts with a higher positive charge on the $ZrCl_2$ fragments. Intuitively, higher charged polymerization species should allow for easier β-hydride elimination, thus facilitating the series of eliminations/insertions that lead to chain epimerization.[18,38,92,94]

https://dx.doi.org/10.1021/acs.macromol.0c01771
Macromolecules XXXX, XXX, XXX−XXX

When chain epimerization becomes a competitive process, it rapidly overtakes contributions from enantioselectivity errors; at lower temperatures stereoselectivity is essentially determined by the enantioselectivity, and at higher temperatures by chain epimerization, with a small crossover temperature range (~10−20 °C) separating the two regimes. The temperature at which the crossover happens is catalyst and propene pressure dependent. To truly predict stereoselectivity of a set of catalysts in the crossover range (which is the case here), one would need a dynamic QSAR model, able to penalize only catalysts for which chain epimerization has become dominant. However, even the static model presented earlier (which penalizes all catalysts to some degree) represents an improvement over Cavallo's model,[99] which only accounts for intrinsic catalyst enantioselectivity.

What Makes a Good High-Temperature Propene Polymerization Catalyst? **M18** represents a perfect cautionary tale. Optimized for performance at 60 °C, the catalyst represents the best-known balanced combination (Table 1) of stereoselectivity, regioselectivity, and molar mass capability.[51] This promise fails spectacularly to translate to higher operating temperatures (Table 2). To understand this failure, it is instructive to itemize the temperature response imparted by different substituent patterns (Table 5).

Table 5. Substituent Patterns and Their Individual Effects on Temperature Sensitivity

temperature response	regioselectivity	stereoselectivity	molar mass capability
poor	4-(3,5-R_2Ph)	4-(2-MePh)	6-*i*Pr
		4-(*N*-carbazolyl)	5-OMe
		4-(3,5-TMS_2Ph)	4-Ph
		2-Et	2-Et
		4-(2-thienyl)	4-(2-thienyl)
		4-(2-furyl)	4-(2-furyl)
		4-H	4-H
		2-*i*Pr	2-*i*Pr
good	all others	5-R	4-(3,5-R_2Ph)
		4-(3,5-*t*Bu_2Ph)	4-(2-MePh)
		4-phenyl	6-*t*Bu
		6-R	5-OMe + 6-*t*Bu
		7-OMe	5-Me
			4-(*N*-carbazolyl)

A strong regioselectivity temperature response is imparted by 4-(3,5-R_2Ph) substituents (R = *t*Bu or TMS). Bulky R groups in *meta* positions of the 4-Ph primarily affect the TS leading to regioerrors via backside tuning.[51] However, small changes in orientation of the 4-Ph can have significant effects on the position of the remote R groups ("lever effect").

A strong stereoselectivity temperature response often goes along with substituents that increase the electrophilicity of the central metal, like 4-(2-MePh), 4-(*N*-carbazolyl), 2-Et, 2-*i*Pr, or 4-(2-thienyl), as judged by the NPA charge on the $ZrCl_2$ fragment (Table 6) and the success of the previously introduced QSAR model. Conversely, substituents decreasing the electrophilicity like 6-R, 5-R, and 4-(3,5-*t*Bu_2Ph) show good temperature sensitivity. This being said, electronic effects do not seem to be solely responsible, with the rather poor performance of **M1** being an obvious example.

The rigidity of the metallocene appears to also play a role. We have recently demonstrated that fine-tuning of the Ind-Ph dihedral angle via placement of substituents on the 5-position of the rigid indenyl fragment (hard lock) or the *ortho* positions of the flexible substituent (soft lock) on the rigid backbone can increase stereoselectivity.[50,51] Hard locks appear to offer an advantage at higher temperatures over soft locks. As a matter of fact, the poor temperature response of the 4-(2-MePh) fragment in **M5** is nearly unaffected by placement of an electron donating 6-*t*Bu group in **M13**.

Table 6. NPA Charges on the $ZrCl_2$ Fragment for Complexes M1−M21[a]

ID	substituent pattern	q^-_{ZrCl2}
M1	2-Me	0.390
M9	2-Me-4-(3,5-*t*Bu_2Ph)-7-OMe	0.397
M12	2-Me-4-(3,5-*t*Bu_2Ph)-6-*t*Bu	0.398
M6	2,5-Me-4-Ph	0.399
M10	2-Me-4-Ph-5-OMe-6-*t*Bu	0.400
M17	2-Me-4-(3,5-*t*Bu_2Ph)-6-Me	0.401
M8	2-Me-4-Ph-6-*t*Bu	0.403
M7	2-Me-4-Ph-6-*i*Pr	0.404
M13	2-Me-4-(2-MePh)-6-*t*Bu	0.405
M20	2-Me-4-(3,5-TMS_2Ph)	0.407
M4	2-Me-4-(3,5-*t*Bu_2Ph)	0.408
M18	2-Et-4-(3,5-*t*Bu_2Ph)-6-Me	0.410
M11	2-Me-4-(2-thienyl)-6-*t*Bu	0.410
M19	2-Me-4-Ph-5-OMe	0.412
M2	2-Me-4-Ph	0.412
M5	2-Me-4-(2-MePh)	0.414
M21	2-Me-4-(2-furyl)	0.415
M3	2-Me-4-(2-thienyl)	0.418
M16	2-Me-4-(*N*-carbazolyl)	0.419
M15	2-Et-4-Ph	0.422
M14	2-*i*Pr-4-Ph	0.430

[a]Catalysts are ordered by increasing charge, q^-_{ZrCl2} (in e^-).

Molar mass capability temperature sensitivity appears to be largely independent of electronic effects, with substituents increasing the electrophilicity of the metal (e.g., 4-(*N*-carbazolyl), 2-Et, and 2-*i*Pr) being found on different ends of the spectrum. The corresponding QSAR model also does not use an electronic descriptor. Rather, it appears that the most dramatic temperature effects are tied to substituents with greater rotational flexibility, most notably 6-*i*Pr or 2-Et; those two-faced substituents present either more or less steric hindrance to the active pocket. Electronically, 6-*i*Pr and 6-*t*Bu have nearly identical effects, but 6-*i*Pr has a much worse temperature response. Both hard and soft locks (*vide supra*) appear to be beneficial for molar mass capability at higher temperatures.

The poor high-temperature performance of **M18** thus becomes understandable. **M18** maximizes the use of rather flexible substituent motifs (2-Et and 4-(3,5-*t*Bu_2Ph)) and electronic tuning, an approach that backfires at higher temperatures.

In light of the above discussion, the following generalizations can be made regarding design principles for high temperature, high performance bis(indenyl)zirconocenes: (a) Any flexibility in the catalyst backbone should be avoided. "Ambiguous" substituents allowing for orientations that relieve steric hindrance from the active pocket in any way can lead to dramatic performance drops for one or more of the experimental performance indicators. (b) Electron-donating substituents can improve the stereoselectivity response at high

https://dx.doi.org/10.1021/acs.macromol.0c01771
Macromolecules XXXX, XXX, XXX−XXX

temperature, but this comes invariably at the expense of lower regioselectivity. (c) Bulky substituents in the 6-position can increase molar mass capability, but the downside is similar to (b), a decreased regioselectivity.

The two-faced effects of using (b) or (c) disqualifies both approaches. Contrarily, enhancing the rigidity comes with no apparent downside. Rieger has introduced the concept of ultrarigidity with **M9**—which has been shown to produce nearly perfect iPP (in its Hf derivative) at low polymerization temperatures[54,103]—arguing that the rigidity imparted by the 7-OMe substituents and the 3,5-*t*Bu groups is chiefly responsible for the improved performance. However, in light of the present results, **M9** appears to not be rigid enough for good performance at 100 °C. Also, Nifant'ev's **M10** with the 4-Ph ring hard-locked into position by the adjacent 5-OMe as well as **M6** (5-Me) group use this increased rigidity approach.[104] **M6** shows by far the best temperature response.

Increasing rigidity via "locks" that hinder rotation of substituents as used in **M10** and **M6** has only rarely been exploited. In light of the results presented in this paper, we believe that further "stiffening" of ultrarigid metallocenes might offer avenues to high-performance, high-temperature stable zirconocenes.

CONCLUSION

We have screened a library of 21 C_2-symmetric zirconocenes for their performance in propene polymerization at a relatively high polymerization temperature of 100 °C. Together with earlier published data for 60 °C, this allowed for the first time for a broad systematic analysis of how temperature-sensitive substituent effects are at higher polymerization temperature. While all catalysts show a performance decrease, the extent of it varies depending on the substituent pattern. Regioselectivity is barely affected, but stereoselectivity and molar mass capability are heavily affected.

The experimental database was used to build QSAR models using a set of previously established 3D steric and one electronic descriptor. Models trained at 60 °C for regioselectivity and molar mass capability could be easily transferred. At higher polymerization temperatures chain epimerization can substantially contribute to the observed stereoselectivity. A simple QSAR model relying on one 3D-steric descriptor that captures the enantioselectivity of the catalyst and an electronic descriptor that captures the propensity for chain epimerization was developed. To our knowledge, this is the first time that a model has been proposed capturing both stereoerror sources.

Decreased electrophilicity of the metal was found to be beneficial for stereoselectivity; it is, however, detrimental to high regioselectivity. Critical analysis of the temperature stability of the various substituent effects showed that catalysts of higher rigidity experience less dramatic performance drops at higher temperature, and increasing said rigidity above current levels appears to be a possible avenue to further improve the performance.

ASSOCIATED CONTENT

Supporting Information

The Supporting Information is available free of charge at https://pubs.acs.org/doi/10.1021/acs.macromol.0c01771.

Polymerization conditions and polymer analysis, QSAR descriptor details, QSAR models, analysis of variance for QSAR models, leave-one-out analysis for QSAR models (PDF)

$LMCl_2$ structures (XYZ)

AUTHOR INFORMATION

Corresponding Authors

Roberta Cipullo − *Dipartimento di Scienze Chimiche, Università di Napoli Federico II, 80126 Napoli, Italy; DPI, 5600 AX Eindhoven, The Netherlands;* orcid.org/0000-0003-3846-1999; Email: r.cipullo@unina.it

Dmitry V. Uborsky − *Department of Chemistry, Lomonosov Moscow State University, 119991 Moscow, Russia; DPI, 5600 AX Eindhoven, The Netherlands*; Email: duborsky@med.chem.msu.ru

Christian Ehm − *Dipartimento di Scienze Chimiche, Università di Napoli Federico II, 80126 Napoli, Italy; DPI, 5600 AX Eindhoven, The Netherlands;* orcid.org/0000-0002-2538-5141; Email: christian.ehm@unina.it

Authors

Antonio Vittoria − *Dipartimento di Scienze Chimiche, Università di Napoli Federico II, 80126 Napoli, Italy; DPI, 5600 AX Eindhoven, The Netherlands;* orcid.org/0000-0003-3178-7427

Georgy P. Goryunov − *Department of Chemistry, Lomonosov Moscow State University, 119991 Moscow, Russia; DPI, 5600 AX Eindhoven, The Netherlands;* orcid.org/0000-0002-5188-5799

Vyatcheslav V. Izmer − *Department of Chemistry, Lomonosov Moscow State University, 119991 Moscow, Russia; DPI, 5600 AX Eindhoven, The Netherlands*

Dmitry S. Kononovich − *Department of Chemistry, Lomonosov Moscow State University, 119991 Moscow, Russia; DPI, 5600 AX Eindhoven, The Netherlands*

Pavel S. Kulyabin − *Department of Chemistry, Lomonosov Moscow State University, 119991 Moscow, Russia; DPI, 5600 AX Eindhoven, The Netherlands*

Rocco Di Girolamo − *Dipartimento di Scienze Chimiche, Università di Napoli Federico II, 80126 Napoli, Italy; DPI, 5600 AX Eindhoven, The Netherlands;* orcid.org/0000-0001-8815-2997

Peter H. M. Budzelaar − *Dipartimento di Scienze Chimiche, Università di Napoli Federico II, 80126 Napoli, Italy; DPI, 5600 AX Eindhoven, The Netherlands;* orcid.org/0000-0003-0039-4479

Alexander Z. Voskoboynikov − *Department of Chemistry, Lomonosov Moscow State University, 119991 Moscow, Russia; DPI, 5600 AX Eindhoven, The Netherlands*

Vincenzo Busico − *Dipartimento di Scienze Chimiche, Università di Napoli Federico II, 80126 Napoli, Italy; DPI, 5600 AX Eindhoven, The Netherlands*

Complete contact information is available at: https://pubs.acs.org/10.1021/acs.macromol.0c01771

Notes

The authors declare no competing financial interest.

ACKNOWLEDGMENTS

This research forms part of the research program of DPI, project 800.

https://dx.doi.org/10.1021/acs.macromol.0c01771
Macromolecules XXXX, XXX, XXX−XXX

■ ABBREVIATIONS

iPP, isotactic polypropylene; QSAR, quantitative structure−reactivity relationship; HTE, high-throughput experimentation; M_w = weight, averaged molecular weight; M_n, number-averaged molecular weight; NMR, nuclear magnetic resonance; $\%V_{Bur}$, percentage of buried volume; T_p, polymerization temperature; T_m, melting point; MAO, methylaluminoxane; mLLDPE, metallocence linear low-density polyethylene; TTB, $[trityl]^+[B(C_6F_5)_4]^-$; GPC, gel permeation chromatography; PDI, polydispersity index; (M_w/M_n), $regio_{tot}$ total fraction of 2,1 and 3,1 monomeric units in % (^{13}C NMR); 1-σ, fraction of stereoirregular monomeric units in % (^{13}C NMR), according to the enantiomorphic-site statistical model; NPA, natural population analysis.

■ REFERENCES

(1) Natta, G.; Pino, P.; Mazzanti, G.; Giannini, U. A Crystallizable Organometallic Complex Containing Titanium And Aluminum. *J. Am. Chem. Soc.* **1957**, *79*, 2975−2976.

(2) Breslow, D. S.; Newburg, N. R. Bis-(Cyclopentadienyl)-Titanium Dichloride —Alkylaluminum Complexls As Catalysts For The Polymerization Of Ethylene. *J. Am. Chem. Soc.* **1957**, *79*, 5072−5073.

(3) Sinn, H.; Kaminsky, W.; Vollmer, H.-J.; Woldt, R. Living Polymers" on Polymerization with Extremely Productive Ziegler Catalysts. *Angew. Chem., Int. Ed. Engl.* **1980**, *19*, 390−392.

(4) Kaminsky, W.; Külper, K.; Brintzinger, H. H.; Wild, F. R. W. P. Polymerization of Propene and Butene with a Chiral Zircono-cene and Methylalumoxane as Cocatalyst. *Angew. Chem., Int. Ed. Engl.* **1985**, *24*, 507−508.

(5) Long, W. P.; Breslow, D. S. Der Einfluß von Wasser auf die katalytische Aktivität von Bis(π-cyclopentadienyl)titandichlorid-Dimethylaluminiumchlorid zur Polymerisation von Äthylen. *Liebigs Ann.* **1975**, *1975*, 463−469.

(6) Andresen, A.; Cordes, H.-G.; Herwig, J.; Kaminsky, W.; Merck, A.; Mottweiler, R.; Pein, J.; Sinn, H.; Vollmer, H.-J. Halogen-Free Soluble Ziegler Catalysts for the Polymerization of Ethylene. Control of Molecular Weight by Choice of Temperature. *Angew. Chem., Int. Ed. Engl.* **1976**, *15*, 630−632.

(7) Gahleitner, M.; Resconi, L.; Doshev, P. Heterogeneous Ziegler-Natta, metallocene, and post-metallocene catalysis: Successes and challenges in industrial application. *MRS Bull.* **2013**, *38*, 229−233.

(8) Tullo, A. H. Metallocenes Rise Again. *Chem. Eng. News* **2010**, *88*, 10−16.

(9) Ali, S. Polyolefin Catalyst Market Overview. *Catal. Rev.* **2014**, *27*, 7.

(10) Shamiri, A.; Chakrabarti, M.; Jahan, S.; Hussain, M.; Kaminsky, W.; Aravind, P.; Yehye, W. The Influence of Ziegler-Natta and Metallocene Catalysts on Polyolefin Structure, Properties, and Processing Ability. *Materials* **2014**, *7*, 5069.

(11) Pasquini, N., Ed.; *Polypropylene Handbook*, 2nd ed.; Hanser Publishers: Munich, 2005.

(12) Cecchin, G.; Morini, G.; Piemontesi, F.; Seidel, A. *Kirk-Othmer Encyclopedia of Chemical Technology*; Wiley-Interscience: New York, 2007; Vol. *26*, pp 502−554.

(13) Rappé, A. K.; Skiff, W. M.; Casewit, C. J. Modeling Metal-Catalyzed Olefin Polymerization. *Chem. Rev.* **2000**, *100*, 1435−1456.

(14) Möhring, P. C.; Coville, N. J. Group 4 metallocene polymerisation catalysts: quantification of ring substituent steric effects. *Coord. Chem. Rev.* **2006**, *250*, 18−35.

(15) Bochmann, M. Cationic Group 4 metallocene complexes and their role in polymerisation catalysis: the chemistry of well defined Ziegler catalysts. *J. Chem. Soc., Dalton Trans.* **1996**, 255−270.

(16) Mülhaupt, R. Catalytic Polymerization and Post Polymerization Catalysis Fifty Years After the Discovery of Ziegler's Catalysts. *Macromol. Chem. Phys.* **2003**, *204*, 289−327.

(17) Brintzinger, H. H.; Fischer, D.; Mülhaupt, R.; Rieger, B.; Waymouth, R. M. Stereospecific Olefin Polymerization with Chiral Metallocene Catalysts. *Angew. Chem., Int. Ed. Engl.* **1995**, *34*, 1143−1170.

(18) Busico, V.; Cipullo, R. Microstructure of polypropylene. *Prog. Polym. Sci.* **2001**, *26*, 443−533.

(19) Ewen, J. A. Mechanisms of stereochemical control in propylene polymerizations with soluble Group 4B metallocene/methylalumoxane catalysts. *J. Am. Chem. Soc.* **1984**, *106*, 6355−6364.

(20) Ewen, J. A. Symmetry rules and reaction mechanisms of Ziegler−Natta catalysts1. *J. Mol. Catal. A: Chem.* **1998**, *128*, 103−109.

(21) Resconi, L.; Cavallo, L.; Fait, A.; Piemontesi, F. Selectivity in Propene Polymerization with Metallocene Catalysts. *Chem. Rev.* **2000**, *100*, 1253−1346.

(22) Stehling, U.; Diebold, J.; Kirsten, R.; Roell, W.; Brintzinger, H. H.; Juengling, S.; Muelhaupt, R.; Langhauser, F. *ansa*-Zirconocene Polymerization Catalysts with Anelated Ring Ligands - Effects on Catalytic Activity and Polymer Chain Length. *Organometallics* **1994**, *13*, 964−970.

(23) Jüngling, S.; Mülhaupt, R.; Stehling, U.; Brintzinger, H.-H.; Fischer, D.; Langhauser, F. The role of dormant sites in propene polymerization using methylalumoxane activated metallocene catalysts. *Macromol. Symp.* **1995**, *97*, 205−216.

(24) Zurek, E.; Ziegler, T. Toward the Identification of Dormant and Active Species in MAO (Methylaluminoxane)-Activated, Dimethylzirconocene-Catalyzed Olefin Polymerization. *Organometallics* **2002**, *21*, 83−92.

(25) Landis, C. R.; Sillars, D. R.; Batterton, J. M. Reactivity of Secondary Metallocene Alkyls and the Question of Dormant Sites in Catalytic Alkene Polymerization. *J. Am. Chem. Soc.* **2004**, *126*, 8890−8891.

(26) Busico, V.; Cipullo, R.; Romanelli, V.; Ronca, S.; Togrou, M. Reactivity of Secondary Metal−Alkyls in Catalytic Propene Polymerization: How Dormant Are "Dormant Chains"? *J. Am. Chem. Soc.* **2005**, *127*, 1608−1609.

(27) Flisak, Z.; Ziegler, T. Dormant" secondary metal-alkyl complexes are not omnipresent. *Proc. Natl. Acad. Sci. U. S. A.* **2006**, *103*, 15338−15342.

(28) van Leeuwen, P. W. N. M.; Chadwick, J. C. Dormant Species in Transition Metal-Catalyzed Olefin Polymerization. In *Homogeneous Catalysts*; Wiley-VCH Verlag GmbH & Co. KGaA: 2011; pp 131−150.

(29) Gibson, V. C.; Spitzmesser, S. K. Advances in Non-Metallocene Olefin Polymerization Catalysis. *Chem. Rev.* **2003**, *103*, 283−316.

(30) Baier, M. C.; Zuideveld, M. A.; Mecking, S. Post-Metallocenes in the Industrial Production of Polyolefins. *Angew. Chem., Int. Ed.* **2014**, *53*, 9722−9744.

(31) Ziegler, K.; Holzkamp, E.; Breil, H.; Martin, H. Polymerisation von Äthylen und anderen Olefinen. *Angew. Chem.* **1955**, *67*, 426−426.

(32) Natta, G.; Pino, P.; Corradini, P.; Danusso, F.; Mantica, E.; Mazzanti, G.; Moraglio, G. Crystalline High Polymers Of α-Olefins. *J. Am. Chem. Soc.* **1955**, *77*, 1708−1710.

(33) Busico, V. Giulio Natta and the Development of Stereoselective Propene Polymerization. *Adv. Polym. Sci.* **2013**, *257*, 37.

(34) *Introduction to Industrial Polypropylene Properties, Catalysts, Processes*; Malpass, D. B., Band, E. I., Eds.; Scrievener Publishing LLC: 2012; p 154.

(35) Severn, J. R.; Chadwick, J. C.; Duchateau, R.; Friederichs, N. "Bound but Not Gagged" Immobilizing Single-Site α-Olefin Polymerization Catalysts. *Chem. Rev.* **2005**, *105*, 4073−4147.

(36) Boussie, T. R.; Diamond, G. M.; Goh, C.; Hall, K. A.; LaPointe, A. M.; Leclerc, M. K.; Murphy, V.; Shoemaker, J. A. W.; Turner, H.; Rosen, R. K.; Stevens, J. C.; Alfano, F.; Busico, V.; Cipullo, R.; Talarico, G. Nonconventional Catalysts for Isotactic Propene Polymerization in Solution Developed by Using High-Throughput-Screening Technologies. *Angew. Chem., Int. Ed.* **2006**, *45*, 3278−3283.

(37) Busico, V.; Cipullo, R. Influence of Monomer Concentration on the Stereospecificity of 1-Alkene Polymerization Promoted by C_2-

https://dx.doi.org/10.1021/acs.macromol.0c01771
Macromolecules XXXX, XXX, XXX−XXX

symmetric *ansa*-Metallocene Catalysts. *J. Am. Chem. Soc.* **1994**, *116*, 9329−9330.
(38) Busico, V.; Cipullo, R.; Caporaso, L.; Angelini, G.; Segre, A. L. C_2-symmetric ansa-metallocene catalysts for propene polymerization: Stereoselectivity and enantioselectivity. *J. Mol. Catal. A: Chem.* **1998**, *128*, 53−64.
(39) Yoder, J. C.; Bercaw, J. E. Chain Epimerization during Propylene Polymerization with Metallocene Catalysts: Mechanistic Studies Using a Doubly Labeled Propylene. *J. Am. Chem. Soc.* **2002**, *124*, 2548−2555.
(40) Leclerc, M. K.; Brintzinger, H. H. ansa-Metallocene derivatives. 31. Origins of stereoselectivity and stereoerror formation in *ansa*-zirconocene-catalyzed isotactic propene polymerization. A deuterium labeling study. *J. Am. Chem. Soc.* **1995**, *117*, 1651−1652.
(41) Wester, T. S.; Johnsen, H.; Kittilsen, P.; Rytter, E. The effect of temperature on the polymerization of propene with dimethylsilylbis(1-indenyl)zirconium dichloride/methylaluminoxane and dimethylsilylbis(2-methyl-1-indenyl)zirconium dichloride/methyl-aluminoxane. Modeling of kinetics. *Macromol. Chem. Phys.* **1998**, *199*, 1989−2004.
(42) Reichelt, K.; Parkinson, M.; Resconi, L. Influence of Temperature on the Regioselectivity of Highly Isospecific C_2-Symmetric Zirconocenes in Propene Polymerization. *Macromol. Chem. Phys.* **2016**, *217*, 2415−2430.
(43) Falivene, L.; Cavallo, L.; Talarico, G. Buried Volume Analysis for Propene Polymerization Catalysis Promoted by Group 4 Metals: A Tool for Molecular Mass Prediction. *ACS Catal.* **2015**, *5*, 6815−6822.
(44) Nifant'ev, I. E.; Ivchenko, P. V.; Bagrov, V. V.; Churakov, A. V.; Mercandelli, P. 5-Methoxy-Substituted Zirconium Bis-indenyl ansa-Complexes: Synthesis, Structure, and Catalytic Activity in the Polymerization and Copolymerization of Alkenes. *Organometallics* **2012**, *31*, 4962−4970.
(45) Resconi, L.; Focante, F.; Balboni, D.; Nifant'ev, I.; Ivchenko, P.; Bagrov, V. (Basell) International Patent Application WO116034, 2007.
(46) Resconi, L.; Castro, P.; Huhtanen, L. (Borealis) International Patent Application WO135004, 2011.
(47) Resconi, L.; Castro, P.; Huhtanen, L.; Hafner, N. (Borealis) International Patent Application WO135005, 2011.
(48) Izmer, V. V.; Lebedev, A. Y.; Kononovich, D. S.; Borisov, I. S.; Kulyabin, P. S.; Goryunov, G. P.; Uborsky, D. V.; Canich, J. A. M.; Voskoboynikov, A. Z. *ansa*-Metallocenes Bearing 4-(N-Azolyl)-2-methylindenyl and Related Ligands: Development of Highly Isoselective Catalysts for Propene Polymerization at Higher Temperatures. *Organometallics* **2019**, *38*, 4645−4657.
(49) Spaleck, W.; Kueber, F.; Winter, A.; Rohrmann, J.; Bachmann, B.; Antberg, M.; Dolle, V.; Paulus, E. F. The Influence of Aromatic Substituents on the Polymerization Behavior of Bridged Zirconocene Catalysts. *Organometallics* **1994**, *13*, 954−963.
(50) Ehm, C.; Vittoria, A.; Goryunov, G. P.; Kulyabin, P. S.; Budzelaar, P. H. M.; Voskoboynikov, A. Z.; Busico, V.; Uborsky, D. V.; Cipullo, R. Connection of Stereoselectivity, Regioselectivity, and Molecular Weight Capability in *rac*-$R'_2Si(2\text{-Me-4-R-indenyl})_2ZrCl_2$ Type Catalysts. *Macromolecules* **2018**, *51*, 8073−8083.
(51) Ehm, C.; Vittoria, A.; Goryunov, P. G.; Izmer, V. V.; Kononovich, S. D.; Samsonov, V. O.; Di Girolamo, R.; Budzelaar, P. H. M.; Voskoboynikov, Z. A.; Busico, V.; Uborsky, V. D.; Cipullo, R. An Integrated High Throughput Experimentation/Predictive QSAR Modeling Approach to *ansa*-Zirconocene Catalysts for Isotactic Polypropylene. *Polymers* **2020**, *12*, 1005.
(52) Izmer, V. V.; Lebedev, A. Y.; Nikulin, M. V.; Ryabov, A. N.; Asachenko, A. F.; Lygin, A. V.; Sorokin, D. A.; Voskoboynikov, A. Z. Palladium-Catalyzed Pathways to Aryl-Substituted Indenes: Efficient Synthesis of Ligands and the Respective *ansa*-Zirconocenes. *Organometallics* **2006**, *25*, 1217−1229.
(53) Voskoboynikov, A. Z.; Nikulin, M. V.; Ryabov, A. N.; Lygin, A. V.; Coker, C. L.; Canich, J. A. M. US Pat. US7910783.
(54) Schöbel, A.; Herdtweck, E.; Parkinson, M.; Rieger, B. Ultra-Rigid Metallocenes for Highly Iso- and Regiospecific Polymerization of Propene: The Search for the Perfect Polypropylene Helix. *Chem. - Eur. J.* **2012**, *18*, 4174−4178.
(55) Fujita, T.; Fukuoka, O.; Imuda, J.; Kawai, K.; Kiso, Y.; Nitahara, M.; Saito, J.; Tashiro, K.; Ueda, T.; Yoshida, M. New Transition Metal Compound, olefin Polymerization Catalyst Component Comprising the Same, Olefin Polymerization Catalyst containing this Component and Polymerization of Olefin. Japanese Patent JPH07286005A, 31 October 1995.
(56) Busico, V.; Cipullo, R.; Mingione, A.; Rongo, L. Accelerating the Research Approach to Ziegler−Natta Catalysts. *Ind. Eng. Chem. Res.* **2016**, *55*, 2686−2695.
(57) Busico, V.; Pellecchia, R.; Cutillo, F.; Cipullo, R. High-Throughput Screening in Olefin-Polymerization Catalysis: From Serendipitous Discovery Towards Rational Understanding. *Macromol. Rapid Commun.* **2009**, *30*, 1697−1708.
(58) Vittoria, A.; Meppelder, A.; Friederichs, N.; Busico, V.; Cipullo, R. Demystifying Ziegler−Natta Catalysts: The Origin of Stereoselectivity. *ACS Catal.* **2017**, *7*, 4509−4518.
(59) Vittoria, A.; Busico, V.; Cannavacciuolo, F. D.; Cipullo, R. Molecular Kinetic Study of "Chain Shuttling" Olefin Copolymerization. *ACS Catal.* **2018**, *8*, 5051−5061.
(60) Vittoria, A.; Mingione, A.; Abbate, R. A.; Cipullo, R.; Busico, V. High Throughput Experimentation Protocol for Quantitative Measurements of Regioselectivity in Ziegler−Natta Polypropylene Catalysis. *Ind. Eng. Chem. Res.* **2019**, *58*, 14729−14735.
(61) Cuthbert, E. N. T.; Vittoria, A.; Cipullo, R.; Busico, V.; Budzelaar, P. H. M. Structure-Activity Relationships for Bis(phenolate-ether) Zr/Hf Propene Polymerization Catalysts. *Eur. J. Inorg. Chem.* **2020**, *2020*, 541−550.
(62) Uborsky, D. V.; Mladentsev, D. Y.; Guzeev, B. A.; Borisov, I. S.; Vittoria, A.; Ehm, C.; Cipullo, R.; Hendriksen, C.; Friederichs, N.; Busico, V.; Voskoboynikov, A. Z. C_1-Symmetric Si-bridged (2-indenyl)(1-indenyl) ansa-metallocenes as efficient ethene/1-hexene copolymerization catalysts. *Dalton Trans.* **2020**, *49*, 3015−3025.
(63) Ehm, C.; Vittoria, A.; Goryunov, G. P.; Izmer, V. V.; Kononovich, D. S.; Samsonov, O. V.; Budzelaar, P. H. M.; Voskoboynikov, A. Z.; Busico, V.; Uborsky, D. V.; Cipullo, R. On the limits of tuning comonomer affinity of 'Spaleck-type' ansa-zirconocenes in ethene/1-hexene copolymerization: a high-throughput experimentation/QSAR approach. *Dalton Trans.* **2020**, *49*, 10162−10172.
(64) Ehm, C.; Mingione, A.; Vittoria, A.; Zaccaria, F.; Cipullo, R.; Busico, V. High-Throughput Experimentation in Olefin Polymerization Catalysis: Facing the Challenges of Miniaturization. *Ind. Eng. Chem. Res.* **2020**, *59*, 13940−13947.
(65) Song, F.; Cannon, R. D.; Lancaster, S. J.; Bochmann, M. Activator effects in metallocene-based alkene polymerisations: unexpectedly strong dependence of catalyst activity on trityl concentration. *J. Mol. Catal. A: Chem.* **2004**, *218*, 21−28.
(66) Frisch, M. J.; Trucks, G. W.; et al. *Gaussian 16*, Revision A.03; Gaussian, Inc.: Wallingford, CT, 2016. For a full citation, see the Supporting Information.
(67) Baker, J. An Algorithm for the Location of Transition-States. *J. Comput. Chem.* **1986**, *7*, 385−395.
(68) Baker, J. *PQS*, 2.4; Parallel Quantum Solutions: Fayetteville, AR, 2001.
(69) Budzelaar, P. H. M. Geometry optimization using generalized, chemically meaningful constraints. *J. Comput. Chem.* **2007**, *28*, 2226−2236.
(70) Ehm, C.; Budzelaar, P. H. M.; Busico, V. Calculating accurate barriers for olefin insertion and related reactions. *J. Organomet. Chem.* **2015**, *775*, 39−49.
(71) Tao, J. M.; Perdew, J. P.; Staroverov, V. N.; Scuseria, G. E. Climbing the density functional ladder: Nonempirical meta-generalized gradient approximation designed for molecules and solids. *Phys. Rev. Lett.* **2003**, *91*, 146401.
(72) Balabanov, N. B.; Peterson, K. A. Systematically convergent basis sets for transition metals. I. All-electron correlation consistent

https://dx.doi.org/10.1021/acs.macromol.0c01771
Macromolecules XXXX, XXX, XXX−XXX

basis sets for the 3d elements Sc−Zn. *J. Chem. Phys.* **2005**, *123*, 064107.
(73) Balabanov, N. B.; Peterson, K. A. Basis set limit electronic excitation energies, ionization potentials, and electron affinities for the 3d transition metal atoms: Coupled cluster and multireference methods. *J. Chem. Phys.* **2006**, *125*, 074110.
(74) Schuchardt, K. L.; Didier, B. T.; Elsethagen, T.; Sun, L.; Gurumoorthi, V.; Chase, J.; Li, J.; Windus, T. L. Basis Set Exchange: A Community Database for Computational Sciences. *J. Chem. Inf. Model.* **2007**, *47*, 1045−1052.
(75) Schwerdtfeger, P. The Pseudopotential Approximation in Electronic Structure Theory. *ChemPhysChem* **2011**, *12*, 3143−3155.
(76) Peterson, K. A.; Figgen, D.; Dolg, M.; Stoll, H. Energy-consistent relativistic pseudopotentials and correlation consistent basis sets for the 4d elements Y−Pd. *J. Chem. Phys.* **2007**, *126*, 124101.
(77) Zhao, Y.; Truhlar, D. G. The M06 suite of density functionals for main group thermochemistry, thermochemical kinetics, noncovalent interactions, excited states, and transition elements: two new functionals and systematic testing of four M06-class functionals and 12 other functionals. *Theor. Chem. Acc.* **2008**, *120*, 215−241.
(78) Ehm, C.; Cipullo, R.; Budzelaar, P. H. M.; Busico, V. Role(s) of TMA in polymerization. *Dalton Trans.* **2016**, *45*, 6847−6855.
(79) Zaccaria, F.; Ehm, C.; Budzelaar, P. H. M.; Busico, V. Accurate Prediction of Copolymerization Statistics in Molecular Olefin Polymerization Catalysis: The Role of Entropic, Electronic, and Steric Effects in Catalyst Comonomer Affinity. *ACS Catal.* **2017**, *7*, 1512−1519.
(80) Zaccaria, F.; Cipullo, R.; Budzelaar, P. H. M.; Busico, V.; Ehm, C. Backbone rearrangement during olefin capture as the rate limiting step in molecular olefin polymerization catalysis and its effect on comonomer affinity. *J. Polym. Sci., Part A: Polym. Chem.* **2017**, *55*, 2807−2814.
(81) Ehm, C.; Cipullo, R.; Passaro, M.; Zaccaria, F.; Budzelaar, P. H. M.; Busico, V. Chain Transfer to Solvent in Propene Polymerization with Ti Cp-phosphinimide Catalysts: Evidence for Chain Termination via Ti−C Bond Homolysis. *ACS Catal.* **2016**, *6*, 7989−7993.
(82) Ehm, C.; Budzelaar, P. H. M.; Busico, V. Metal−carbon bond strengths under polymerization conditions: 2,1-insertion as a catalyst stress test. *J. Catal.* **2017**, *351*, 146−152.
(83) Zaccaria, F.; Ehm, C.; Budzelaar, P. H. M.; Busico, V.; Cipullo, R. Catalyst Mileage in Olefin Polymerization: The Peculiar Role of Toluene. *Organometallics* **2018**, *37*, 2872−2879.
(84) Ehm, C.; Budzelaar, P. H. M.; Busico, V. Tuning the Relative Energies of Propagation and Chain Termination Barriers in Polyolefin Catalysis through Electronic and Steric Effects. *Eur. J. Inorg. Chem.* **2017**, *2017*, 3343−3349.
(85) Whitten, J. L. Coulombic potential energy integrals and approximations. *J. Chem. Phys.* **1973**, *58*, 4496.
(86) Baerends, E. J.; Ellis, D. E.; Ros, P. Self-consistent molecular Hartree—Fock—Slater calculations I. The computational procedure. *Chem. Phys.* **1973**, *2*, 41−51.
(87) Feyereisen, M.; Fitzgerald, G.; Komornicki, A. Use of approximate integrals in ab initio theory. An application in MP2 energy calculations. *Chem. Phys. Lett.* **1993**, *208*, 359−363.
(88) Vahtras, O.; Almlöf, J.; Feyereisen, M. W. Integral approximations for LCAO-SCF calculations. *Chem. Phys. Lett.* **1993**, *213* (5), 514−518.
(89) Falivene, L.; Credendino, R.; Poater, A.; Petta, A.; Serra, L.; Oliva, R.; Scarano, V.; Cavallo, L. SambVca 2. A Web Tool for Analyzing Catalytic Pockets with Topographic Steric Maps. *Organometallics* **2016**, *35*, 2286−2293.
(90) Glendening, E. D.; Reed, A. E.; Carpenter, J. E.; Weinhold, F. NBO3.1 ed., Theoretical Chemistry Institute, University of Wisconsin: Madison, WI, 2001.
(91) In one case, the catalysts produced oligomers and the regioselectivity could not be determined.
(92) Busico, V.; Cipullo, R. Growing chain isomerizations in metallocene-catalyzed Ziegler-Natta 1-alkene polymerization. *J. Organomet. Chem.* **1995**, *497*, 113−118.
(93) Busico, V.; Caporaso, L.; Cipullo, R.; Landriani, L.; Angelini, G.; Margonelli, A.; Segre, A. L. Propene Polymerization Promoted by C_2-Symmetric Metallocene Catalysts: From Atactic to Isotactic Polypropene in Consequence of an Isotope Effect. *J. Am. Chem. Soc.* **1996**, *118*, 2105−2106.
(94) Busico, V.; Brita, D.; Caporaso, L.; Cipullo, R.; Vacatello, M. Interfering Effects of Growing Chain Epimerization on Metallocene-Catalyzed Isotactic Propene Polymerization. *Macromolecules* **1997**, *30*, 3971−3977.
(95) De Rosa, C.; Auriemma, F.; Spera, C.; Talarico, G.; Tarallo, O. Comparison between Polymorphic Behaviors of Ziegler−Natta and Metallocene-Made Isotactic Polypropylene: The Role of the Distribution of Defects in the Polymer Chains. *Macromolecules* **2004**, *37*, 1441−1454.
(96) De Rosa, C.; Auriemma, F.; Di Capua, A.; Resconi, L.; Guidotti, S.; Camurati, I.; Nifant'ev, I. E.; Laishevtsev, I. P. Structure−Property Correlations in Polypropylene from Metallocene Catalysts: Stereodefective, Regioregular Isotactic Polypropylene. *J. Am. Chem. Soc.* **2004**, *126*, 17040−17049.
(97) De Rosa, C.; Auriemma, F.; Resconi, L. Influence of Chain Microstructure on the Crystallization Kinetics of Metallocene-Made Isotactic Polypropylene. *Macromolecules* **2005**, *38*, 10080−10088.
(98) De Rosa, C.; Auriemma, F.; Paolillo, M.; Resconi, L.; Camurati, I. Crystallization Behavior and Mechanical Properties of Regiodefective, Highly Stereoregular Isotactic Polypropylene: Effect of Regiodefects versus Stereodefects and Influence of the Molecular Mass. *Macromolecules* **2005**, *38*, 9143−9154.
(99) Poater, A.; Cavallo, L. Comparing families of olefin polymerization precatalysts using the percentage of buried volume. *Dalton Trans.* **2009**, 8885−8890.
(100) Falivene, L.; Cao, Z.; Petta, A.; Serra, L.; Poater, A.; Oliva, R.; Scarano, V.; Cavallo, L. Towards the online computer-aided design of catalytic pockets. *Nat. Chem.* **2019**, *11*, 872−879.
(101) Cramer, R. D.; Patterson, D. E.; Bunce, J. D. Comparative molecular field analysis (CoMFA). 1. Effect of shape on binding of steroids to carrier proteins. *J. Am. Chem. Soc.* **1988**, *110*, 5959−5967.
(102) Alexander, D. L. J.; Tropsha, A.; Winkler, D. A. Beware of R2: Simple, Unambiguous Assessment of the Prediction Accuracy of QSAR and QSPR Models. *J. Chem. Inf. Model.* **2015**, *55*, 1316−1322.
(103) Machat, M. R.; Lanzinger, D.; Pöthig, A.; Rieger, B. Ultrarigid Indenyl-based Hafnocene Complexes for the Highly Isoselective Polymerization of Propene: Tunable Polymerization Performance Adopting Various Sterically Demanding 4-Aryl Substituents. *Organometallics* **2017**, *36*, 399−408.
(104) In both cases, the regioselectivity is however negatively affected because of (b).

https://dx.doi.org/10.1021/acs.macromol.0c01771
Macromolecules XXXX, XXX, XXX−XXX